AIP Journal of Applied Physics

# Optical profiles with 180 μ m resolution of objects hidden in scattering media

Alessandra Andreoni, Luca Nardo, Adriano Brega, and Maria Bondani

Citation: Journal of Applied Physics **101**, 024921 (2007); doi: 10.1063/1.2431680
View online: http://dx.doi.org/10.1063/1.2431680
View Table of Contents: http://scitation.aip.org/content/aip/journal/jap/101/2?ver=pdfcov
Published by the AIP Publishing



# Optical profiles with 180 $\mu$m resolution of objects hidden in scattering media

Alessandra Andreoni and Luca Nardo[a)]
*Dipartimento di Fisica e Matematica, University of Insubria, Via Valleggio 11, 22100 Como, Italy and CNR-INFM, Unita' di Como, Via Valleggio 11, 22100 Como, Italy*

Adriano Brega
*CNR-INFM, Unita' di Como, Via Valleggio 11, 22100 Como, Italy*

Maria Bondani
*National Laboratory for Ultrafast and Ultraintense Optical Science (ULTRAS)-CNR-INFM, Unita' di Como, Via Valleggio 11, 22100 Como, Italy*

(Received 26 September 2006; accepted 18 November 2006; published online 29 January 2007)

We measure the time-of-flight distributions of near-infrared photons emerging from thick scattering media within a collection angle of 0.6 mrad about the incident light direction by means of a time-correlated single-photon counting apparatus endowed with $<35$ ps resolution. These measurements, which are performed with a picosecond laser beam, allow us to isolate the weakly scattered (ballistic/snake) photons from the multiply scattered ones. By scanning the incidence position across a target we find variations in the fraction of detected unscattered photons that are significative of local changes in the optical parameters of the target. In particular, if either opaque, light diffusing, or transparent objects are embedded in the scattering medium, their profiles can be reconstructed and their nature can be assessed. Opaque objects embedded in realistic tissue phantoms are detected with $<180$ $\mu$m spatial resolution. © *2007 American Institute of Physics*. [DOI: 10.1063/1.2431680]

## I. INTRODUCTION

Ever since 1929, when Cutler published his results on his attempt of performing a transillumination image of human breast,[1] optical imaging of tissues for diagnostic purposes has been one of the principal goals of biomedical optics. The reason of this continuous and lively interest rests in the fact that the presently applied diagnostic techniques, be they based on nuclear magnetic resonance or x-ray tomography, even if assuring millimeter spatial resolutions, fail to offer the tools for large-scale routine clinical exams on healthy patients, both for sanitary and technical-economic reasons. In fact, both classes of techniques are extremely invasive, and patients cannot submit themselves to diagnostic exams without incurring into the risk of contracting side-effect pathologies, including cancer. Moreover, a sanitary staff operating on these technologies chronically undergoes dangerous doses of electromagnetic/ionizing radiation. Finally, the necessary instrumentation is extremely complex and expansive to build, to run, and to keep. This leads to both relevant social costs and lack of diffusion of structures offering this kind of diagnostic facilities, with the consequence of long waiting lists. These issues discourage both physicians from prescribing and healthy patients from submitting to screening. Despite of this, early diagnosis is often propaedeutic to the efficient treatment of severe diseases, and probably a good weapon we have to fight cancer.

Optical imaging, especially with near-infrared light (NIR) (700–1100 nm wavelengths), is a nonionizing procedure, so reasonable doses can be repeatedly employed without any harm to the patient. Moreover, a distinction among different soft tissues (optical biopsy) is in principle possible, due to substantial differences in their way of scattering and absorbing NIR light.

The ultimate spatial resolution allowed by an optical imaging system is constituted by the diffraction limit, and it is thus far beyond 1 mm. Unfortunately, at difference with x rays, NIR light is highly scattered by biological samples, so that on the average a photon is expected to be diffused several times by even a very thin slice of tissue. An amazing afford has been devoted over the past decades both to develop theoretical models capable of reproducing and explaining the main features of NIR light interactions with biological tissues and to experimentally assess the optical parameters of as many biological tissues as possible.

It is now accepted that biological tissues behave, with respect to interaction with light, similarly to dense colloidal dispersions of lipid and protein clusters in water. As for any other turbid and highly scattering optical medium, the easiest way to model their light transmittance is to assume isotropic diffusion. In this limit, the value of the collimated transmittance signal, that is, the fraction of incident light passing through the medium without being scattered, is given by $T=\exp(-\mu L)$, $L$ being the thickness of the medium and $\mu$ the extinction coefficient. For pure isotropic diffusion, $\mu$ is simply the sum of the absorption coefficient $\mu_a$ and of the scattering coefficient $\mu_s$. Photons constituting the collimated transmittance signal have not been scattered; they are called ballistic photons. It is quite intuitive, and generally accepted,

[a)]Author to whom correspondence should be addressed; Fax: +390312386119; electronic mail: luca.nardo@uninsubria.it

 

that if one could select only the ballistic photons emerging from the medium and measure the intensity of the collimated transmittance signal as a function of the incident light position, one could get a map of the variations in the optical properties of the medium (including discontinuities embedded in it) virtually endowed with diffraction-limited spatial resolution.

The anisotropy of the scattering can be accounted for in the frame of the isotropic model by introducing a third parameter, the anisotropy factor $g$, and substituting, in the transmittance equation, the scattering coefficient $\mu_s$ with the reduced scattering coefficient (also called the transport coefficient) $\mu_s'=\mu_s(1-g)$. As the effect of anisotropy is to increase the collimated transmittance signal, the anisotropy coefficient takes values spanning from 0 (completely isotropic diffusion) to 1 (no diffusion). However, in practical situations the signal contains not only ballistic photons but also a number of the so called "snake photons," that is, photons emerging from the sample after having experienced only a limited amount of scattering events. As the snake photons follow a trajectory very close to that of the ballistic ones, they still carry information on the spatial distribution of the optical properties of the imaged specimen, but the ultimate achievable spatial resolution is reduced by a somehow unpredictable amount.

A wide body of both experimental and simulated data is now available regarding the values assumed by $\mu_a$, $\mu_s$, and $g$ in many biological tissues. Zhao *et al.*[2] have reported both literature and personal data on $\mu_a$ and $\mu_s'$ of a chicken muscle and bone tissues for impinging light wavelengths ranging from 633 to 834 nm. Beek *et al.*[3] have published an extensive study on values of $\mu_a$, $\mu_s$, and $g$ for different tissues (cartilage, lung, liver, muscle, myocardium, and skin) of many animals (rabbit, goat, rat, piglet, and dog) at five incident light wavelengths in the range between 630 and 1064 nm. Das *et al.*[4] reported values of the scattering and absorption lengths (the inverse of $\mu_s$ and $\mu_a$, respectively) for a chicken fat and thin breast tissues at 620 nm. Sankaran *et al.*[5] reported the $\mu_s'$ and $g$ values for a myocardial muscle and an adipose tissue of a pig at 633 nm. Troy and Thennadil,[6] Matcher *et al.*,[7] and Simpson *et al.*[8] have accomplished detailed studies on the optical properties of human Caucasian and Negroid skins in the red,[8] near IR,[7,8] and far IR[6] and of human abdominal muscle in the range between 600 and 1000 nm.[8] Finally, two very detailed studies on healthy and diseased human breast tissues have been performed by Pifferi *et al.*[9] and by Peters *et al.*[10] for a wide range of incident light wavelengths spanning from 500 to 1100 nm. Although there is a wide variation in the literature data referred to similar tissues, all these data can be summarized for our purposes in the following observations: $\mu_s$ of biological tissues is very high, typically spanning in the range from 10 to 100 $cm^{-1}$; in the range of wavelength spanning from 600 to 600 to 1100 nm the absorption contribution to the extinction coefficient can be neglected as $\mu_a < 0.01\mu_s$; scattering by biological tissues is highly forward, with $g>0.9$; $\mu_s$ monotonically decreases as a function of light wavelength, while $g$ keeps substantially constant.

Due to the high variability and easy deterioration of biological samples, leading to scarcely reproducible experimental results, many studies have been devoted to find media appropriate for *in vitro* experiments and displaying absorption and scattering characteristics similar to those tissues (tissue phantoms).

Between the end of the 80s and the first half of the 90s, thanks to the enormous progresses registered in laser and light detector technologies, the attempts at performing optical imaging through thick scattering media have multiplied. Plenty of papers issued in this period reported on brilliant strategies to tackle this problem (reviewed by Dunsby and French[11] and by Hebden *et al.*[12]). Almost all these strategies make use of one or more of the following four major selection modes: spatial filtering[13,14] (selection of the collimated transmittance signal by detecting only the light emerging from the sample within a surface corresponding to the incident beam cross sectional area), mode filtering[14] (selection only of the light emerging from the sample in the same direction of the incident beam), time gating[4,14] (selection only of the photons arriving within a certain time limit after illumination of the sample), and coherence-gated imaging[15] (detection only of the light emerging from the sample in phase with the incident light).

Unfortunately, none of these attempts has managed to get rid of the problem of selecting the limited fraction of early arriving (ballistic and snake) photons constituting the sole portion of the light emerging from the sample carrying valid imaging information. This lack of positive results has led many authors to conclude that performing optical imaging of biological tissues thicker than a few millimeters by exploiting the properties of the collimated transmitted signal is simply impossible[11,15] and to concentrate on other strategies implying the analysis of the multiply scattered, dominant part of the emerging light.[2,13,16] These methods are obviously endowed with poor spatial resolution (not better than that pursued with x-ray tomography for realistic tissue phantoms[16,17] and signal-to-noise ratio (S/N).

However, at least in principle, the conclusion that direct transmittance imaging with NIR light is unfeasible is erroneous. In fact, the considerations on the quantum shot-noise limit, which led Hee *et al.*[15] to conclude that with illumination intensities compatible with safe irradiation of *in vivo* tissues the maximum thickness of a medium allowing a sufficient number of weakly scattered early arriving photons to be detected with his heterodyne-based method is about 4 mm, are perfectly correct and widely apply for virtually any other coherence-selection method, but the quantum shot-noise has nothing to do with single-photon detection, even if many authors[11] referred to the Hee *et al.* estimation as to a general detection limit. Both streak cameras and time-correlated single-photon counting (TCSPC) techniques can be utilized to perform time-of-flight (TOF) measurements with a resolution of tens of picoseconds and a sensitivity down to a few/single photons. Let us consider a thought experiment in which a NIR laser beam of an average power $P\approx 200$ mW is made to impinge on a slab of a scattering medium of thickness $L\approx 5$ cm having $\mu_a\approx 0$, $\mu_s\approx 45$ $cm^{-1}$, and $g\approx 0.9$, that could mimic a biological tissue, such as a breast adipose tissue or a myocardial muscle. The collimated

transmittance of the sample is $T \approx \exp(-\mu_s' L) \approx e^{-23} \approx 10^{-10}$, which means that only one photon out of tens of billions impinging on the sample is going to be a ballistic or a snake photon, emerging from the sample without being appreciably scattered. However, the absolute rate of these photons would be given by $dN/dt = TP/h\nu \approx 10^{11}$ photons/s, which is not at all too small one to be measured. This straightforward and simple calculation shows that even if optical imaging is not expectable to be applied indiscriminately for any diagnostic purpose in substitution to the present x-ray and NMR-based techniques, its range of applicability can be extended to several-centimeter-thick tissues. In this range particularly interesting medical and research systems, such as tissues typically dealt with in mammography, endoscopy, or anatomy studies on small animals, fall.

The problem with the detection of early arriving photons is thus not intrinsically related to the lack of sufficiently sensitive detectors but just with devising optical setups being capable of isolating just these photons from the total emerging light signal, though it is composed by an overwhelming number of multiply scattered ones. In 2004,[18] we performed TCSPC measurements on the light emerging from suspensions of Intralipid, which is a scattering medium typically used in medicine as a human-tissue phantom. We used a home-assembled, state of the art excitation-collection-detection apparatus, featuring a picosecond-pulsed, high-repetition-rated, continuous-wave mode-locked Nd: vanadate (VAN) laser emitting 1064 nm pulses at $P \approx 200$ mW average power, a collection lens of diameter $d = 0.3$ cm selecting light in an angle $\alpha = 0.6$ mrad around the incident beam direction, and a TCSPC system endowed with a pulse response $<35$ ps full width at half maximum (FWHM). In this condition, mode and spatial filterings are simultaneously applied to the emerging light: all the nearly unscattered photons are collected by the collection lens and conveyed to the single-photon counter, but, assuming isotropic diffusion and homogeneous spreading of the photon highly scattered in the forward direction over the whole surface of the sample ($S = 20$ cm$^2$), only a fraction of multiply scattered photons given by $F_{\mathrm{Det}} \approx [\pi(\tan\alpha)^2/(4\pi)]\ [\pi(d/2)^2/S] \approx 3.3 \times 10^{-10}$ is conveyed to the detector. Thus, a relative frequency of nearly unscattered photons around 0.3 of the total detected photon flux was to be expected for optical parameters of the scattering medium similar to those of the thought experiment of above ($T \approx 10^{-10}$). In fact, in similar experimental conditions we managed to distinguish a measurable fraction of nearly unscattered photons in the TOF distributions even for optical parameters of the scattering medium of biomedical relevance.[18]

In the present work, one-dimensional (1D) scanning patterns of opaque, light diffusing, and transparent objects, embedded in Intralipid suspensions featuring clinically relevant optical parameters, are presented. Scanning the sample allows us to detect the position and transverse dimension of the embedded objects with spatial resolution definitely better than the value of 1–2 mm, which represents the present limit of medical apparatus. In fact, for opaque objects, we demonstrate a resolution of $\approx 180$ $\mu$m, a value that is virtually limited only by the diameter of the incident beam. Moreover, the profiles are qualitatively different for different optical properties of the embedded object, and exhibit signal-to-noise ratio values (S/N > 20 for opaque objects, $\approx 17$ for the scattering object, and $\approx 18$ for the transparent object) that are much higher than those reported in the literature for

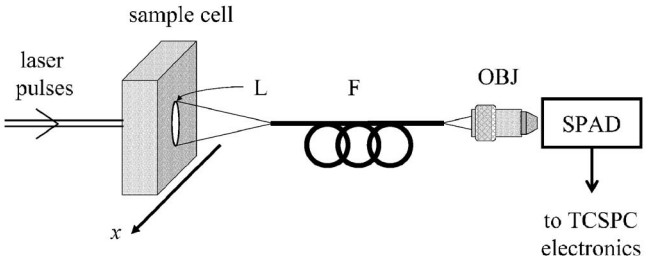


FIG. 1. Experimental apparatus for TOF measurements with time-correlated single-photon counting technique (TCSPC). Collection lens $L$; single-mode fiber $F$; microscope objective (obj); single-photon avalanche diode (SPAD). Lens $L$ is located as near as possible to the cuvette window; the SPAD sensitive surface lies on the image plane.

## II. MATERIALS AND METHODS

### A. Laser and experimental setup

Our system, which is described in detail elsewhere,[18] employs a Nd:VAN mode-locked laser (GE-100-1064-VAN, Time-Bandwidth Products GmbH, Zürich, Switzerland) as the source of pulses at 1064 nm (9 ps duration and 113 MHz repetition rate). As sketched in Fig. 1, the light beyond the sample cell is conveyed by a single-mode fiber $F$ to the detector, which is a single-photon avalanche photodiode (SPAD) of original design.[19,20] The fiber and the collection lens $L$ which are monolithically mounted and kept aligned with the incident beam throughout the measurements, allow collection of light with a 0.6 mrad acceptance angle. The sample cell, a 1 cm thick, 5 cm wide, 4 cm high quartz cuvette, is mounted on a micrometric translation stage ($\frac{1}{2}$ in. course), which displaces it transversally to the beam (see $x$ axis in Fig. 1).

### B. The diffusing medium

The Intralipid (Fresenius Kabi AB, Stockholm, Sweden) is a fluid mixture of proteins and lipids clinically used for the feeding of patients via phleboclysis. Due to its scattering and absorption properties it has been widely used as a tissue phantom in laboratory research on optical imaging.[2,13] The optical parameters of Intralipid in water at many wavelengths in the visible spectrum have been reported in literature. On the contrary, we could find very few data in the near IR. Perhaps the most complete study on the optical properties of Intralipid has been performed by van Staveren *et al.*,[21] who have measured $\mu_s$ and $g$ for a 10% weight-to-volume concentrated suspension of Intralipid as a function of the scattered radiation wavelength in the interval of 400–1000 nm. We interpolated these experimental curves to find reliable values for the two parameters at 1064 nm and calculated $\mu_s \approx 150$ cm$^{-1}$ and $g \approx 0.49$. The reduced scattering coefficient $\mu_s'$ was then assumed to be $\mu_s' = \mu_s(1-g) = 78$ cm$^{-1}$ for such a suspension. Other works report $\mu_s$

variations with respect to Intralipid concentration.[22,23] For 632.8 nm radiation, the trend is almost linear for concentrations well below 10%, while for higher concentrations $\mu_s$ tends to saturate. We assumed a similar behavior at 1064 nm and calculated $\mu_s \approx 50\ \mathrm{cm}^{-1}$ for the ~3% concentrated dispersions we used by linear interpolation from the 10% suspension value. By assuming the value of $g$ to be independent of the Intralipid concentration, we thus calculated $\mu_s' = 25\ \mathrm{cm}^{-1}$. This interpolated value of $\mu_s'$ scales well with those reported at 1064 nm by Troy and Thennadil,[6] that is, $\mu_s' = 18\ \mathrm{cm}^{-1}$, $\mu_s' = 35\ \mathrm{cm}^{-1}$, and $\mu_s' = 56\ \mathrm{cm}^{-1}$, for Intralipid at 2%, 5%, and 10%, respectively.

As we did not consider completely exhaustive the experimental data we found in the literature, we decided to check the value of $\mu_s'$ we inferred in the way we have just described by proceeding to the fit of our TOF distributions to four different purely diffusional models. To do this, we assumed the refraction index of a 3% Intralipid suspension to be equal to 1.33.[22] By using the equation derived by Patterson *et al.*[24] and assuming a pointlike collection of the emergent radiation in correspondence to the center of the incident beam, we obtained the values $\mu_s' = 26\ \mathrm{cm}^{-1}$ and $\mu_a = 0.01\ \mathrm{cm}^{-1}$ for the transport and the absorption coefficients, respectively. The same model corrected by the finite dimension of the collection lens[24] gave $\mu_s' = 25\ \mathrm{cm}^{-1}$ and $\mu_a = 0.01\ \mathrm{cm}^{-1}$. Fitting to the equation derived by Gandjbakhche *et al.*[25] gave $\mu_s' = 23\ \mathrm{cm}^{-1}$ and $\mu_a = 0.01\ \mathrm{cm}^{-1}$, while applying the equation of Kaltenbach and Kaschke[26] we obtained $\mu_s' = 20\ \mathrm{cm}^{-1}$ and $\mu_a = 0.04\ \mathrm{cm}^{-1}$ (note that this last model gives the same results as that of Patterson integrated over the entire output area[24,27]). The considered models give very similar results, compatible with that we inferred by the experimental data reported in the literature. We thus concluded $\mu_s' = 25\ \mathrm{cm}^{-1}$ to be a reliable value for the transport coefficient.

Note that, as reported in the literature,[6,23] the absorption coefficient of Intralipid resulted to be negligible as compared to $\mu_s'$.

### C. The embedded objects

Opaque objects: (i) black-painted metal razor blade, (ii) 4.5 mm diameter cylindrical black-painted metal nail, and (iii) 270 $\mu$m diameter intraderma syringe needle. Transparent object: 4.5 mm diameter cylinder made of Plexiglass. Diffusing object: 4.5 mm diameter cylinder made of Delrin.

Delrin is an acetal resin whose optical properties in the red/NIR have been reported to be similar to those of human breast tissue.[28,29] However, we could find only a few papers reporting optical parameters of Delrin, at visible wavelengths. Gannot *et al.*[30] reported the values $\mu_s' = 16\ \mathrm{cm}^{-1}$ and $\mu_a = 0.08\ \mathrm{cm}^{-1}$ and $\mu_s' = 27\ \mathrm{cm}^{-1}$ and $\mu_a = 0.04\ \mathrm{cm}^{-1}$ for the Delrin transport and absorption coefficient at 488 and at 553 nm, respectively. Sundberg *et al.*[31] measured $\mu_s' = 24.3\ \mathrm{cm}^{-1}$ and $\mu_a = 0.017\ \mathrm{cm}^{-1}$ at 632.8 nm. Finally, Flock *et al.*[32] reported $\mu_s' = 12\ \mathrm{cm}^{-1}$ and $\mu_a = 0.02\ \mathrm{cm}^{-1}$ at 785 nm. Data inferred from independent studies appear to be in substantial conflict to one another. Moreover, even comparison of data reported in the same work leads to the surprising conclusion that the Delrin transport coefficient is not a monotonically decreasing function of wavelength.[31] These discrepancies might be due to the presence, in the Delrin structure, of residual ordered domains on the microscopic scale, leading to a behavior somehow more complicated than that of a liquid scattering medium. Moreover, there actually exist many resins of very different chemical compositions, all produced by DuPont and called Delrin: This makes any comparison particularly hard. We thus decided to try a direct estimation of the optical parameters of our samples. We measured TOF distributions of the late-arriving, highly scattered photons emerging from a 1 cm thick slab made of the same material as the cylinder, by slightly misaligning the collection fiber to prevent detection of the early arriving photons, and fitted them to the equations given by the diffusional models we considered for Intralipid as well. By assuming the constant value of 1.48 for the Delrin refractive index,[31] we found that the values of the absorption coefficient were also virtually constant ($\mu_a = 0.02\ \mathrm{cm}^{-1}$), while the transport coefficient achieved different values from the different models: $\mu_s' = 24\ \mathrm{cm}^{-1}$ from the Patterson equation and pointlike detection, $\mu_s' = 23\ \mathrm{cm}^{-1}$ from the same model and finite dimension of the collection lens,[24] $\mu_s' = 17\ \mathrm{cm}^{-1}$ from the Gandjbakhche equation,[25] and $\mu_s' = 21\ \mathrm{cm}^{-1}$ from the Kaltenbach and Kaschke equation.[26] We thus assumed for the transport coefficient of our Delrin cylinder the value $\mu_s' = 22\ \mathrm{cm}^{-1}$, which corresponds to that of 2.7% Intralipid.

### D. Experimental procedure

The objects are inserted at fixed positions in the quartz cuvette containing appropriate dilutions of 10% Intralipid in de-ionized water. The center of each object is located on the plane halfway between the front and the back windows of the cuvette. Subsequent TOF distributions are collected by moving the sample cell by steps of 1 mm for 2 mm incident beam diameter. Smaller steps of 100–200 $\mu$m are used when the incident beam is narrowed, by using suitable optics (not shown in Fig. 1), down to a waist diameter of ≈0.25 mm with a Rayleigh range greater than the 1 cm cell thickness. In all measurements, the acquisition is stopped when the peak of the TOF distribution reaches 10 000 counts. The maximum acquisition time for a TOF was approximately 1 h.

For each set of TOF distributions corresponding to a scan [counts $C_x(t)$ as a function of time] we also measure the TOF distribution in the absence of object $A(t)$, the TOF distribution for the laser beam passing through the cuvette filled with distilled water $W(t)$, and the TOF distribution of the diffused fraction of the photons $D(t)$. The latter is obtained by timing the photons upon removing the object and slightly misaligning the $L$-plus-$F$ collection system to prevent the collection of the early arriving photons.

### E. Data processing and error evaluation

All TOF distributions are smoothed two times by adjacent averaging over three channels and normalized to their integrals. Each TOF distribution $C_x(t)$ (see the example plotted as gray diamonds in Fig. 2) is fitted to a linear combination $L_x(t;\alpha_x,\beta_x)$ of $W(t)$ and $D(t)$ [that is, $L_x(t;\alpha_x,\beta_x)$

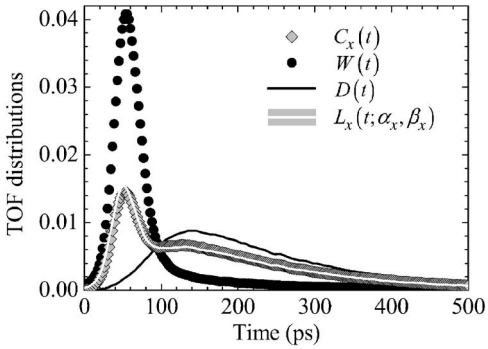


FIG. 2. Experimental TOF distribution for the sample cell filled with 3.3% Intralipid [$C_x(t)$, gray diamonds] and with water [$W(t)$, dots], measured with the fiber aligned and TOF distribution of the purely scattered photons [$D(t)$, black full line], which is measured, for 3.3% Intralipid, by slightly misaligning the light collection fiber. Distributions $C_x(t)$, $W(t)$, and $D(t)$ are normalized to their integrals. The white full line is the best fitting curve $L_x(t;\alpha_x,\beta_x)$ obtained with the procedure described in the text ($\alpha_x$=0.348 and $\beta_x$ =0.652).

$=\alpha_x W(t)+\beta_x D(t)]$ by using a simple home-written MATLAB routine to find the best values of $\alpha_x$ and $\beta_x$. Figure 2 also shows the plots of $W(t)$ (dots), $D(t)$ (black full line), and $L_x(t;\alpha_x,\beta_x)$ (white full line). As the experimental $C_x(t)$ is well recovered by the linear combination $L_x(t;\alpha_x,\beta_x)$, we assume the quantity $p(x)=\alpha_x/(\alpha_x+\beta_x)$ to represent the relative weight of $W(t)$ in $C_x(t)$. Thus $p(x)$ is the probability of a detected photon to have crossed the sample cell by traveling through the water fraction of the scattering medium, that is, being nearly unscattered.

For each scanning position we acquired two subsequent TOF distributions. Each $p(x)$ displayed on the presented scan plots is the average of the values calculated from this two independent and subsequent experimental TOFs. The error is given by the standard deviation. The calculated $p(x)$ are reproduced with $<5\%$ accuracy.

Due to dramatic changes in the photon to water relative weight in a TOF distribution owning to even minimal differences in the alignment of the fiber with respect to the incident laser beam, much larger differences are registered in the $p(x)$ obtained by TOF registered in different measurement sessions.

### F. Definition of spatial resolution and signal-to-noise ratio

The spatial resolution of a transmittance image of a sharp-edge object is usually defined through the following steps:[13,16] First, a linear fit of the points of the image displaying the edge is performed, then the distance between the points of the line whose values correspond to 90% of the out-of-object transmittance and to 10% of the out-of-object transmittance is taken to be the image spatial resolution. In this work we adopt this definition.

We define the S/N as the ratio of the $p(x)$ difference between positions beyond the object and immediately outside of it to the standard deviation $\sigma$ of the background values [values of $p(x)$ measured far aside the obstacle in successive independent TOF distribution acquisitions].

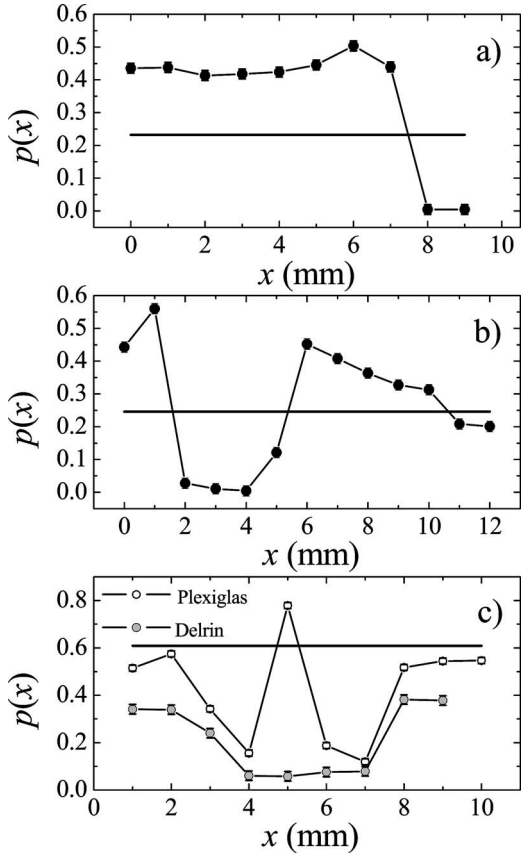


FIG. 3. Photon probabilities of traveling through the medium without being scattered $p(x)$, as calculated from TOF measurements on sample cells containing: (a) the opaque blade, (b) the nail in 3.0% Intralipid, and (c) the 4.5 mm diameter cylinders of Delrin (gray dots) and Plexiglas (open dots) in 2.5% Intralipid. The blade edge is at $x\approx 7$ mm, the opaque nail of 3.5 mm diameter is centered at $x\approx 3.5$ mm, and the Delrin and Plexiglas cylinders of are centered at $x\approx 5$ mm. The horizontal lines mark the background values from the TOF measured after removal of the obstacles. The values of the noise in the measurements are $\sigma\approx 0.015$, $\sigma\approx 0.016$, and $\sigma\approx 0.020$ in (a), (b), and (c), respectively.

## III. RESULTS AND DISCUSSION

We first describe the results of measurements in which the incident beam diameter is 2 mm. Each data plot shown below corresponds to a single scan and the $x$ values are the micrometer readings. When the black-painted razor blade, which darkens the cell up to $\approx 7$ mm from its center, is immersed in 3.0% Intralipid, we find the $p(x)$ values plotted as dots in Fig. 3(a) as a function of $x$. The horizontal line in the figure marks the $p(x)$ value (background value) that we determined from the TOF distribution $A(t)$ measured upon removing the blade. Note that the presence of the opaque obstacle at $x\geqslant 7$ mm gives vanishing $p(x)$ for $x\geqslant 8$ mm whereas $p(x)$ is above the background value at $x\leqslant 7$ mm, that is, at positions for which the beam crosses the cell without hitting the blade we find a $p(x)$ value greater than the one measured for the 3.0% Intralipid samples with no object embedded. Substitution of the blade with the black-painted nail located at $x\approx 3.5$ mm in the same cuvette produces the $p(x)$ that are plotted as dots in Fig. 3(b) together with the value (horizontal line) obtained for $A(t)$. The presence of this opaque cylindrical obstacle produces $p(x)$ values down to about zero in the interval of 2 mm$\leqslant x\leqslant$5 mm. Again, in the

regions next to the nail, $p(x)$ is greater than the background value but, at variance with the case of the blade, $p(x)$ decreases on going far from the nail and approaches the background value at $x>7$ mm. This behavior suggests that the presence of a transversally extended obstacle, such as the blade, obscures the diffused light collected perpendicularly to it even if its edge is definitely aside the line of beam illumination/collection, where it cannot affect the number of early arriving photons. The fact that the diffused photons are obscured only next to the nail, indicates that the nail, as any opaque object (see below), behaves as a transversally extended object only at distances that are small compared to its transverse dimension.

The $p(x)$ plots in Figs. 3(a) and 3(b) can be considered as one-dimensional profiles of the blade and the nail, respectively, with millimeter resolution. In Figs. 3(a) and 3(b), as shown by the error bars, $\sigma \approx 0.015$. As $p(x)$ abruptly falls from 0.45 to 0, we shall state that the objects have been detected with a S/N value $\approx 30$. In the literature we have found only one report concerning imaging of a subcentimeter opaque object immersed in a medium as diffusing as ours: A two-dimensional map, with 2:1 S/N ratio, was obtained as the intensity map of the phase conjugate of the optical field emerging from the sample.[33]

Figure 3(c) shows the $p(x)$ plots for cylinders made of Plexiglas and Delrin as open and gray dots, respectively, together with the background value. These scans represent a preliminary test of the capability of our system to detect translucent samples. The cylinders were located at $x \approx 5$ mm in the cell containing 2.5% Intralipid. The presence of the Delrin obstacle, having a $\mu_s'$ value only $\approx 1.1$ times greater than that of the surrounding medium, produces $p(x)$ values down to about 0.05 in the interval of $3\ \text{mm} \leqslant x \leqslant 7$ mm, while in the outer region we observe a roughly constant $p \approx 0.35$ both next to the Delrin cylinder and relatively far from it (data not shown). As $\sigma \approx 0.020$, these results allow us to detect the Delrin cylinder with $S/N \approx 17$. For the sake of comparison we mention that phantoms with scattering coefficient ratios similar to ours were reported to be at the edge of detectability in a very accurate study of temporal point spread functions measured by a streak camera in a gate of 300 ps time duration.[32] In agreement with other authors,[14,34] we think that the concomitance of high time resolution and small collection angle play a key role in our case. Results of the scanning of a 2.5% Intralipid suspension with the Plexiglas cylinder embedded are plotted in Fig. 3(c). At the position corresponding to the center of the rod ($x \approx 5$ mm), we find a $p$ value of 0.78, which is greater than that determined for the surrounding medium (0.61). A similar central peak of transmission was previously reported for empty cylindrical holes in a Delrin slab.[16] When the line of beam illumination/collection hits the Plexiglas cylinder borders, we find $p<0.61$, which could be probably attributed to refraction index effects at the Intralipid/Plexiglas interface. Even in this last case we can detect the obstacle with $S/N \approx 18$ and assess its dimensions.

The presented data also allow us to distinguish among objects with different optical properties. At the central positions beyond cylindrical objects, the $p(x)$ probability vanishes for the opaque object, whereas it displays a nonzero minimum for the diffusing obstacle and a maximum for the transparent one. In the region immediately outside any of the opaque objects, $p(x)$ is always higher than the value for the pure Intralipid suspension, which is recovered only when the object is relatively far aside. By contrast $p(x)$ starts taking a constant value immediately outside the Delrin obstacle. However, this value is lower than that for the pure 2.5% Intralipid surrounding the obstacle, probably because the insertion of the Delrin cylinder corresponds to the substitution of a volume of 2.5% Intralipid with an equal volume of 2.7% Intralipid equivalent, which makes the sample overall more diffusing. Finally we note that $p(x)$ almost recovers the value of the surrounding medium as soon as the beam avoids hitting the transparent Plexiglas cylinder.

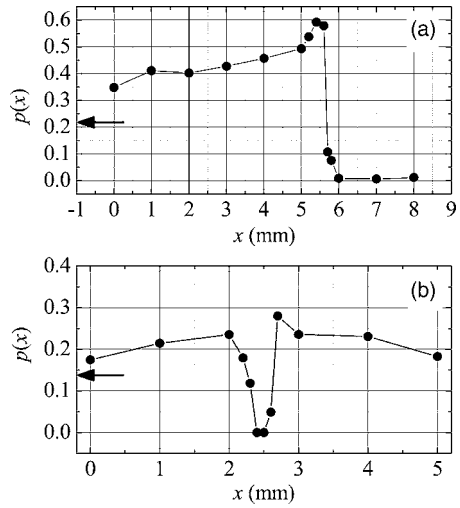


FIG. 4. Probabilities $p(x)$ as calculated from TOF measurements on sample cells containing the opaque blade in 3.3% Intralipid in (a) and a 270 $\mu$m diameter syringe needle in highly concentrated Intralipid (see text) in (b). The arrows mark the background $p$ values: 0.22 in (a) and 0.14 in (b). The values of the noise in the two measurements are $\sigma \approx 0.023$ and $\sigma \approx 0.011$.

At last we present the experiments we made to test the ultimate spatial resolution of both our apparatus and data analysis method in the detection of opaque objects. For these experiments we used an incident beam of $\approx 0.25$ mm FWHM diameter. We repeated the measurements on the black-painted razor blade in 3.3% Intralipid and obtained the $p(x)$ plotted in Fig. 4(a), in which the arrow marks the value determined upon removal of the blade (0.22). The figure shows that the edge of the blade is detected with an accuracy of $\approx 100$ $\mu$m. As already observed in Fig. 3(a), when the line of beam illumination/collection does not hit the obstacle, $p(x)$ is about twice that for the pure surrounding medium even at positions that are distant from the obstacle. We finally performed measurements on a syringe needle of 270 $\mu$m diameter immersed in Intralipid, and increased the Intralipid concentration until $p(x)$ at the obstacle edges was such as to give a $S/N \approx 20$ [data reported in Fig. 4(b)], which we established to be a more than sufficient one. For such an Intralipid suspension, in the absence of the needle, $p=0.14$ [see arrow in Fig. 4(b)]. The results displayed in Fig. 4(b)) still allow us to localize the needle profile and assess its transverse dimension with $<180$ $\mu$m spatial resolution.

## IV. CONCLUSIONS

We measured TOF distributions of the light emerging from highly diffusing suspensions of Intralipid in water, containing objects of different shapes and nature, by a TCSPC technique allowing to collect only photons emerging within an angle of ≈0.6 mrad about incidence and to time them with <35 ps resolution. We developed a method to calculate the relative frequencies $p(x)=\alpha_x/(\alpha_x+\beta_x)$ of early arriving photons. From the values obtained upon scanning the samples, we could derive the position and the transverse dimension of the embedded objects with a spatial resolution (<180 $\mu$m) and a signal to noise ratio (>17) better than those we found in literature for any other attempt of measurements on similar samples. Our method to extract the profiles of embedded objects from the TOF distributions of a scan does not make use of any theoretical model capable of forecasting the shapes of the TOF distributions (it is not an indirect image-reconstruction method). It is rather based on the ability to evaluate the probability of a photon in the forward-directed emerging signal to have crossed the sample cell without experiencing substantial scattering. Based on our results, in principle we might detect discontinuities of sizes as small as 200 $\mu$m in 1–5 cm thick human tissues, which would be relevant for early tumor diagnosis. Moreover, we found qualitatively different profiles for transparent, diffusing, and opaque objects. Thus, we think that assessments on the nature of discontinuities revealed in tissues (e.g., adipose cysts, hydrocysts, or cell clusters) could also be at reach of our method.[9]

The main drawback of our apparatus in its actual version is the long acquisition time we need to perform a scan of few centimeters, but we feel confident that in the future a suitable technology could be devised to allow simultaneous collection on reasonable areas, for example, by means of two-dimensional microarrays of collection fibers. This would make the tomography time be limited only by the time needed to collect the slowest growing TOF distributions, which are those displaying very few early arriving photons.

It took us approximately 1 h, at the mentioned laser powers, to get the distributions in correspondence to the iron blade (purely diffused photons). It must be pointed out, anyway, that the rate of timing in our setup is limited by the dead time of the multichannel board, which can acquire data at a maximum rate of approximately 15 kHz. As we have shown in the Introduction, the expected total rate of early arriving photons for a perfectly nondissipative collection/transduction system and an ideal detector is $\approx 10^{11}$ Hz in our experimental conditions. Even assuming the very low detection efficiency of 0.001 (limited quantum efficiency of the detector and poor coupling to its small sensitive area), we could detect $\approx 10^8$ early arriving photons per second out of an overall (scattered and unscattered) light signal that is ten times more intense (see Introduction). Working in single-photon regime with ≈100 MHz excitation compels us to limit the overall counting rate to no more than a few megahertz. Nevertheless, using state-of-the-art acquisition boards capable to convert timing data with rates of several megahertz would allow us to reduce the acquisition time by 100 times (<1 min per fiber in the microarray). Moreover, as the signal-to-noise ratio of our images is very high, one could easily get statistically reliable information even stopping the collection of the TOF distributions after a smaller number of counting events, for example, at 1000 instead of 10 000 peak channel counts. This would allow us to approximately reduce the acquisition time to few seconds per pixel, which sounds more reasonable as the duration of a clinical exam. Also, a stronger spatial selection of the collimated transmission signal by using collecting lenses of much smaller diameter (≈200 $\mu$m), which is compulsory if we want to conserve submillimeter spatial resolution even adopting collection bundles of lenses and fibers, would decrease the overall counting rate but increase the early arriving photon fraction (see Introduction), further reducing the acquisition time in any case except for pure diffusion (that is, in correspondence of opaque discontinuities at the interior of the scanned tissues). These technical improvements would also allow the measurement system to respect the maximum permissible exposure[35] time for safe irradiation of patients, while the system described in this paper does not fit this specification.

To conclude, we are perfectly aware that a concrete application of the proposed imaging method in medical diagnostics is far away to come, but we think that the expected results of this technique are worth the complex engineering work necessary to its future implementation.

## ACKNOWLEDGMENTS

The authors are grateful to S. Cova and A. S. Spinelli (Politecnico, Milano, Italy) for their support with the instrumentation and to G. Zambra (Como) for the technical assistance.

[1] M. Cutler, Surg. Gynecol. Obstet. **48**, 721 (1929).
[2] H. Zhao, F. Gao, Y. Tanikawa, Y. Onodera, M. Ohmi, M. Haruna, and Y. Yamada, Phys. Med. Biol. **47**, 1979 (2002).
[3] J. F. Beek, P. Blokland, P. Posthumus, M. Aalders, J. W. Pickering, H. J. C. M. Sterenborg, and M. J. C. van Gemert, Phys. Med. Biol. **42**, 2255 (1997).
[4] B. B. Das, K. M. Yoo, and R. R. Alfano, Opt. Lett. **18**, 1092 (1993).
[5] V. Sankaran, M. J. Everett, D. J. Maitland, and J. T. Walsh, Jr., Opt. Lett. **24**, 1044 (1999).
[6] T. L. Troy and S. N. Thennadil, J. Biomed. Opt. **6**, 167 (2001).
[7] S. J. Matcher, M. Cope, and D. T. Delpy, Appl. Opt. **36**, 386 (1997).
[8] C. R. Simpson, M. Kohl, M. Essenpreis, and M. Cope, Phys. Med. Biol. **43**, 2465 (1998).
[9] A. Pifferi, J. Swartling, E. Chikoidze, A. Torricelli, P. Taroni, A. Bassi, S. Andersson-Engels, and R. Cubeddu, J. Biomed. Opt. **9**, 1143 (2004).
[10] V. G. Peters, D. R. Wyman, M. S. Patterson, and G. L. Frank, Phys. Med. Biol. **35**, 1317 (1990).
[11] C. Dunsby and P. M. W. French, J. Phys. D **36**, R207 (2003), and references therein.
[12] J. C. Hebden, S. R. Arridge, and D. T. Delpy, Phys. Med. Biol. **42**, 825 (1997).
[13] J. C. Haselgrove, N. G. Wang, and B. Chance, Med. Phys. **19**, 17 (1992).
[14] K. M. Yoo and R. R. Alfano, Opt. Lett. **15**, 320 (1990).
[15] M. R. Hee, J. A. Izatt, J. M. Jacobson, and J. G. Fujimoto, Opt. Lett. **18**, 950 (1993).
[16] J. C. Hebden, D. J. Hall, and D. T. Delpy, Med. Phys. **22**, 201 (1995).
[17] J. A. Moon, R. Mahon, M. D. Duncan, and J. Reintjes, Opt. Lett. **18**, 1591 (1993).
[18] A. Andreoni, M. Bondani, A. Brega, F. Paleari, A. S. Spinelli, and G. Zambra, Appl. Phys. Lett. **84**, 2457 (2004).
[19] A. L. Lacaita, M. Ghioni, and S. Cova, Electron. Lett. **25**, 841 (1989).
[20] M. Bondani, D. Redaelli, A. Spinelli, A. Andreoni, G. Roberti, P. Riccio,

R. Liuzzi, and I. Rech, J. Opt. Soc. Am. B **20**, 2383 (2003).
[21]H. J. van Staveren, C. J. M. Moes, J. Van Marle, S. A. Prahl, and M. J. C. van Gemert, Appl. Opt. **30**, 4507 (1991).
[22]A. Giusto, R. Saija, M. A. Iatì, P. Denti, F. Borghese, and O. I. Sindoni, Appl. Opt. **42**, 4375 (2003).
[23]G. Zaccanti, S. Del Bianco, and F. Martelli, Appl. Opt. **42**, 4023 (2003).
[24]M. S. Patterson, B. Chance, and B. C. Wilson, Appl. Opt. **28**, 2331 (1989).
[25]A. H. Gandjbakhche, G. H. Weiss, R. F. Bonner, and R. Nossal, Phys. Rev. E **48**, 810 (1993).
[26]J. M. Kaltenbach and M. Kaschke, in *Medical Optical Tomography: Functional Imaging and Monitoring* SPIE Institute Series Vol. IS11, edited by G. Mueller, B. Chance, R. R. Alfano, S. Arridge, J. Beuthan, E. Gratton, M. Kaschke, B. Masters, S. Svanberg, and P. van der Zee (SPIE, Bellingham, Washington, 1993), pp. 65–85.
[27]I. Delfino, M. Lepore, and P. L. Indovina, Appl. Opt. **38**, 4228 (1999).
[28]R. Berg, S. Andersson-Engels, O. Jarlman, and S. Svanberg, Appl. Opt. **35**, 3432 (1996).
[29]S. Fantini *et al.*, in *OSA TOPS on Advances in Optical Imaging and Photon Migration*, edited by R. R. Alfano and J. G. Fujimoto (Optical Society of America, Washington, D.C. 1996), Vol. 2, pp. 160–163.
[30]I. Gannot, R. F. Bonner, G. Gannot, P. C. Fox, P. D. Smith, and A. H. Gandjbakhche, Med. Phys. **25**, 1139 (1998).
[31]M. Sundberg, T. Lindbergh, and T. Strömberg, Proc. SPIE **6084**, 608404 (2006).
[32]S. T. Flock, S. L. Jacques, B. C. Wilson, W. M. Star, and M. J. C. van Gemert, Lasers Surg. Med. **12**, 510 (1992).
[33]G. Le Tolguenec, F. Devaux, and E. Lantz, Opt. Lett. **24**, 1047 (1999).
[34]D. J. Hall, J. C. Hebden, and D. T. Delpy, Appl. Opt. **36**, 7270 (1997).
[35]For Europe see EN 60825-1.